# Immunomodulatory effects of PI3Kδ inhibition in solid tumors – evaluation in a randomized phase II trial

**Christian Ottensmeier** (C.Ottensmeier@liverpool.ac.uk)
University of Liverpool https://orcid.org/0000-0003-3619-1657
**Simon Eschweiler**
La Jolla Institute for Immunology
**Ciro Ramirez Suastegui**
La Jolla Institute for Immunology
**Emma King**
University of Southampton
**Lindsey Chudley**
University of Liverpool
**Jaya Thomas**
University of Southampton
**Wood Oliver**
University of Southampton
**Adrian von Witzleben2**
University of Southampton
**Danielle Jeffrey**
University of Southampton
**Katy McCann**
University of Southampton
**Hayley Simon**
La Jolla Institute for Immunology
**Monalisa Mondal**
La Jolla Institute for Immunology
**Alice Wang**
La Jolla Institute for Immunology
**Elena Lopez-Guadamillas**
University College London
**Yingcong Li**
La Jolla Institute for Immunology
**Nicola Dobbs**

Cancer Research UK
**Louisa Essame**
Cancer Research UK
**Gary Acton**
Cancer Research UK
**Fiona Kelly**
Cancer Research UK
**Gavin Halbert8**
University of Strathclyde
**Joseph Sacco**
University of Liverpool
**Andrew Schache**
University of Liverpool
**Richard Shaw**
University of Liverpool
**James McCaul**
Queen Elizabeth University Hospital
**Claire Paterson**
Beatson West of Scotland Cancer Centre
**Joseph Davies**
Dorset Cancer Centre
**Peter Brennan**
Queen Alexandra Hospital
**Rabindra Rabindra P Singh**
Southampton University Hospitals NHS Foundation Trust
**Paul Loadman**
Institute of Cancer Therapeutics
**William Wilson**
Cancer Research UK & UCL Cancer Trials Centre
**Allan Hackshaw**
University College London
**Klaus Okkenhaug**
University of Cambridge https://orcid.org/0000-0002-9432-4051
**Gareth Thomas**
University of Southampton
**Terry Jones**
University of Liverpool
**Ferhat Ay**
La Jolla Institute For Immunology https://orcid.org/0000-0002-0708-6914

**Greg Friberg**
Amgen
**Bart Vanhaesebroeck**
UCL Cancer Institute https://orcid.org/0000-0002-7074-3673
**Pandurangan Vijayanand**
La Jolla Institute For Immunology https://orcid.org/0000-0001-7067-9723

---

**Biological Sciences - Article**

**Keywords:** Phosphoinositide 3-kinase δ (PI3Kδ), immunotherapy, TREG cells

**Posted Date:** March 19th, 2021

**DOI:** https://doi.org/10.21203/rs.3.rs-337290/v1



---

**Version of Record:** A version of this preprint was published at Nature on May 4th, 2022. See the published version at https://doi.org/10.1038/s41586-022-04685-2.

**Immunomodulatory effects of PI3Kδ inhibition in solid tumors – evaluation in a randomized phase II trial**

Simon Eschweiler[1], Ciro Ramírez-Suástegui[1], Emma King[2,3], Lindsey Chudley[4], Jaya Thomas[2], Oliver Wood[2], Adrian von Witzleben[2], Danielle Jeffrey[2], Katy McCann[2], Hayley Simon[1], Monalisa Mondal[1], Alice Wang[1], Elena Lopez-Guadamillas[5], Yingcong Li[1,6], Nicola A Dobbs[7], Louisa Essame[7], Gary Acton[7], Fiona Kelly[7], Gavin Halbert[8], Joseph J Sacco[4,9], Andrew Graeme Schache[4,10], Richard Shaw[4,10], James Anthony McCaul[11], Claire Paterson[12], Joseph H. Davies[3], Peter A Brennan[13], Rabindra P Singh[14], Paul Loadman[15], William Wilson[16], Allan Hackshaw[16], Klaus Okkenhaug[17], Gareth J. Thomas[2], Terry M. Jones[4,10], Ferhat Ay[1], Greg Friberg[18], Bart Vanhaesebroeck[5], Pandurangan Vijayanand[1,*], Christian H. Ottensmeier[1,2,4, 9,*,&]

[1]La Jolla Institute for Immunology, La Jolla, CA, USA
[2]CRUK and NIHR Experimental Cancer Medicine Center, University of Southampton, Southampton, UK
[3]Dorset Cancer Centre, Poole Hospital NHS Foundation Trust, Poole, UK
[4]Liverpool Head and Neck Center & Institute of Systems, Molecular and Integrative Biology University of Liverpool, Liverpool, UK
[5]UCL Cancer Institute, University College London, London, UK
[6]Division of Biological Sciences, University of California San Diego, La Jolla, CA, USA
[7]Centre for Drug Development (CDD), Cancer Research UK, London, UK
[8]Cancer Research UK Formulation Unit, University of Strathclyde, Glasgow, UK
[9]Clatterbridge Cancer Centre NHS Foundation Trust, Liverpool, UK
[10]Liverpool University Hospitals NHS Foundation Trust, Liverpool, UK
[11]Queen Elizabeth University Hospital, Glasgow, UK
[12]Beatson West of Scotland Cancer Centre, Glasgow, UK
[13]Queen Alexandra Hospital, Portsmouth, UK
[14]Southampton University Hospitals NHS Foundation Trust, Southampton, UK
[15]Institute of Cancer Therapeutics, Bradford, UK
[16]Cancer Research UK & UCL Cancer Trials Centre, London, UK
[17]Department of Pathology, University of Cambridge, UK
[18]Amgen Inc, Thousand Oaks, CA, USA
*jointly supervised and lead this work
[&]Corresponding author

**Abstract**

Phosphoinositide 3-kinase δ (PI3Kδ) plays a key role in lymphocytes and inhibitors targeting this PI3K have been approved for hematological malignancies. While studies in hematological and solid tumor models in mice have demonstrated that PI3Kδ inhibitors (PI3Kδi) can induce anti-tumor immunity, the impact of PI3Kδi on solid tumors in humans remains unclear. Here, we assessed the effects of the PI3Kδi AMG319 in patients with resectable head and neck cancer in a neoadjuvant, double-blind, placebo-controlled randomised phase-II trial. We find that PI3Kδ inhibition decreases tumor-infiltrating immunosuppressive $T_{REG}$ cells and causes heightened cytotoxic potential of tumor-infiltrating $CD8^+$ and $CD4^+$ T cells. Loss of intratumoral $T_{REG}$ cells and an increase in the frequency of activated $T_{REG}$ cells in the blood post-treatment are indicative of systemic effects on $T_{REG}$ tissue retention and maintenance. At the tested AMG319 doses, immune-related adverse events caused treatment discontinuation in 12/21 of AMG319-treated patients, further suggestive of systemic effects on $T_{REG}$ cells. Consistent with this notion, in a murine syngeneic tumor model, PI3Kδi decreased $T_{REG}$ cells in both tumor and non-malignant tissues and affected $T_{REG}$ subtype composition, maintenance and functionality. Our data demonstrate the cancer-immunotherapy potential of PI3Kδ inhibition in humans, but its modulation will need to be carefully balanced to harness its anti-tumor capacity while minimizing immune related toxicity.

## Introduction

Among the PI3K isoforms, PI3Kδ is highly expressed in all leukocytes. PI3Kδ is critical for B-cell antigen receptor (BCR) signaling, facilitating B-cell activation, survival and proliferation, through activation of downstream kinases such as Protein Kinase B (AKT) and the mechanistic target of rapamycin (mTOR) complex 1 (reviewed in Ref.[1]). PI3Kδ inhibitors (PI3Kδi), such as idelalisib, have been approved for the treatment of B-cell malignancies chronic lymphocytic leukemia (CLL) and follicular lymphoma, where the malignant cells are reliant on BCR signaling[2–4]. PI3Kδ also plays a role in T-cell differentiation, migration and function[5,6] by modulating T-cell antigen receptor (TCR) signaling and repression of FOXO transcription factors[1], which in turn regulate genes involved in cell trafficking such as *Klf2, S1pr1* and *Ccr7*[7]. Interestingly, T regulatory ($T_{REG}$) cells seem more sensitive to PI3Kδ inhibition than other T cell subsets, such as cytotoxic $CD8^+$ T cells, which appear largely unaffected in preclinical studies[8–10] and in idelalisib-treated CLL patients[11,12]. In B-cell malignancies, indirect evidence suggests that PI3Kδi-mediated immune-related adverse events (irAEs) such as colitis, hepatotoxicity and pneumonitis[12,13] may be related to the effects of PI3Kδ inhibition on $T_{REG}$ cells (reviewed in Ref.[4,14]). Accordingly, an extensive body of preclinical and clinical studies has shown that disruptions of the PI3Kδ-Foxo1 pathway primarily affect $T_{REG}$ cells[5,10,11,15] by exerting effects that impact $T_{REG}$ cell proliferation[10], survival[16], suppressive capacity[17,18] and tissue residency[7]. These findings imply that the preferential inhibition of $T_{REG}$ cells by PI3Kδi can rebalance the host immune system to induce anti-tumor immune responses and tumor regression, even if cancer cells do not express PI3Kδ. This $T_{REG}$-centric immunomodulatory effect is thus distinct and independent from the effects of blocking PI3Kδ signaling in malignant cells[8–10,19–24]. Similarly, the expression of Foxo1 in $T_{REG}$ cells can promote anti-tumor activity[7], suggesting that PI3Kδi impairs $T_{REG}$ function by de-repressing Foxo1 activity.

To start evaluating the potential for PI3Kδ inhibitors as immunotherapeutic agents in human solid cancers, we administered the PI3Kδi AMG319 to treatment-naive patients with resectable head and neck squamous cell carcinoma (HNSCC) in a neoadjuvant, double-blind,

placebo-controlled randomized phase II trial. AMG319 had an immunomodulatory impact that is remarkably consistent with preclinical data in mice and also aligns with immunomodulatory effects observed in human B-cell malignancies. Our data show that PI3Kδ inhibition in human tumor tissue modulates T cell activities in a manner consistent with enhanced anti-tumor immune responses. Surprisingly however, toxicity profiles (onset and frequency of irAEs) differed from a previous study of AMG319 in B cell malignancies[25], suggesting that alternative dosing regimens will be required to effectively and safely exploit the immunomodulatory impact of PI3Kδ inhibition in human solid cancers.

**PI3Kδ inhibition drives systemic $T_{REG}$ cell depletion**

We initiated our studies by testing the impact of a PI3Kδi in a mouse solid tumour model, performing a more extensive T cell profiling than in any other study to date. C57BL/6 wild-type mice were inoculated with the syngeneic B16F10-OVA melanoma tumor cell line and treated with the previously described PI3Kδi PI-3065[7]. Consistent with previous studies[8,9], we found a significant decrease in tumor volume (**Extended Data Fig. 1a**), even if PI3Kδi treatment was initiated in a therapeutic setting once tumors had become palpable (**Fig. 1a**). The reduction in tumor volume was accompanied by a significant decrease in intratumoral $T_{REG}$ cells (**Fig. 1b**). At the same time, intratumoral $CD8^+$ T cells were significantly increased in frequency, expressed higher levels of PD-1 and exhibited higher proliferative capacity and cytotoxic potential (**Fig. 1c-f**). Tox, a transcription factor recently identified as critical for adaptation and survival of $CD8^+$ T cells in the tumor microenvironment (TME)[26], was also increased post-PI3Kδi (**Fig. 1g**). Notably and contrary to previous reports[27,28], we found that the expression of both GzmB and Ki-67 was almost exclusively limited to $Tox^+CD8^+$ T cells (**Fig. 1h**), demonstrating that these cells, despite showing high expression of PD-1 and Tox, are not functionally exhausted in this tumor model. Thus, the PI3Kδi-induced reduction in intratumoral $T_{REG}$ cells correlated with augmented anti-tumor $CD8^+$ T cell responses. To assess whether PI3Kδ inhibition acts locally within the tumor tissue or systemically *i.e.*, also affecting other non-malignant organs, we performed flow-cytometric analyses of $T_{REG}$ cells in

spleen, tumor and colonic tissue of tumor-bearing FoxP3-RFP reporter mice. Importantly, in PI3Kδi-treated mice, but not placebo-treated control mice, we found a significant decrease in $T_{REG}$ cells in all assessed tissues, indicative of systemic effects of PI3Kδi on $T_{REG}$ maintenance or survival (**Extended Data Fig. 1b**).

**Colonic $T_{REG}$ cells are sensitive to PI3Kδ inhibition**

Since colitis is one of the major irAEs in patients receiving PI3Kδi[4,12,13], we hypothesized that $T_{REG}$ cells present in colonic tissue may be especially sensitive to PI3Kδi. To test this hypothesis in an unbiased manner, we performed single-cell RNA-sequencing of $T_{REG}$ cells isolated from tumor, spleen (lymphoid organ) and colonic tissue of PI3Kδi- and placebo-treated B16F10-OVA tumor-bearing FoxP3-RFP reporter mice. Unbiased clustering analysis depicted by uniform manifold approximation and projection (UMAP) analysis identified 10 $T_{REG}$ cell clusters, implying substantial $T_{REG}$ cell heterogeneity and tissue adaptations (**Fig. 2a-c)**. In agreement with previous studies[29,30] and based on their unique transcriptomic signatures, tissue $T_{REG}$ cells (tumor, colon) clustered distinctly from one another and from lymphoid organ $T_{REG}$ cells (spleen), suggesting the existence of several distinct $T_{REG}$ subtypes in different locations (**Fig. 2a and Extended Data Fig. 2a,b**). Colonic $T_{REG}$ cells exhibited the most pronounced differences between PI3Kδi and placebo treatment, with 869 differentially expressed genes, while splenic and tumor $T_{REG}$ cells exhibited fewer differences (**Fig. 2d-f and Extended Data Table 1**). We also found major changes in the composition of colonic $T_{REG}$ subsets, but not splenic or intratumoral $T_{REG}$ subsets (**Fig. 2b,c** and **Extended Data Fig. 2c**). Two of the colonic $T_{REG}$ subsets (clusters 2 and 8) were depleted in PI3Kδi-treated mice (**Fig. 2b,c** and **Extended Data Fig. 2c**). Cluster 2 colonic $T_{REG}$ cells were enriched for the expression of *Ctla4* and genes encoding chemokine receptors (*Ccr1, Ccr2, Ccr4*), critical for their suppressive[31,32] and migratory[33] capacity, respectively (**Fig. 2g, Extended Data Fig.2d** and **Extended Data Table 2**). Cluster 8 colonic $T_{REG}$ cells resembled the recently described tissue-resident ST2 $T_{REG}$ cells[34–36], which are critical for the protection against chronic inflammation and facilitation of tissue repair. Accordingly, we found enrichment

in the expression of the ST2 $T_{REG}$ signature genes *Il1rl1* (encoding for IL-33R), *Gata3* and *Id2*, as well as of several genes associated with highly suppressive effector $T_{REG}$ cells (*Klrg1, Cd44, Cd69, Pdcd1, Areg, Nr4a1, Il10* and *Tgfb1*) (**Fig. 2g** and **Extended Data Table 2**). While colonic $T_{REG}$ cells in cluster 0 and cluster 8 shared this ST-2 signature, cells in cluster 8 were also enriched for transcripts linked to cellular activation (*Cd44, Icos* and *Klrg1*) and superior suppressive capacity (*Ctla4, Il10 and Gzmb*) (**Fig. 2h**). While the $T_{REG}$ cell clusters (2 and 8) with highly suppressive properties were depleted in PI3Kδi-treated mice, cluster 5 $T_{REG}$ cells, which were enriched in PI3Kδi-treated mice, showed higher expression of several interferon-related response genes (*Stat1, Stat3, Ifrd1*)[37,38], suggestive of a pro-inflammatory environment (**Fig. 2g** and **Extended Data Table 2**). Further corroborating the diverse effects of PI3Kδ inhibition on $T_{REG}$ cells in different tissues, we observed a significant increase of $CD8^+$ T cells in colonic, but not splenic tissue (**Extended Data Fig. 2e,f**). Moreover, these colonic $CD8^+$ T cells expressed higher levels of PD-1 and ICOS upon PI3Kδ inhibition (**Extended Data Fig. 2g,h**), implying treatment-related changes to cell activation, presumably mediated by the $T_{REG}$ cell alterations**.** Taken together, these findings suggest a heightened sensitivity of certain colonic $T_{REG}$ subsets to PI3Kδi, potentially related to the high incidence of colitis observed in patients treated with PI3Kδ inhibitors such as idelalisib.

**Systemic effects of PI3Kδ inhibition in HNSCC patients are associated with the occurrence of irAEs**

In order to explore how our findings above translate to humans, we conducted a multicenter, placebo-controlled phase II neoadjuvant trial with the PI3Kδi AMG319 in resectable HNSCC, with primary study endpoints of safety and changes in the density of $CD8^+$ T cells (**Fig. 3a** and https://www.clinicaltrialsregister.eu/ctr-search/trial/2014-004388-20/results). We focused on Human Papilloma Virus (HPV)-negative HNSCC, as this cancer type is more prevalent, and because patients with this cancer type have poorer outcomes when compared to HPV-positive HNSCC, likely due to overall lower tumor infiltrating lymphocyte (TIL) infiltration[39–41]. Patients were recruited after initial diagnosis and before

definitive surgical treatment (**Extended Data Table 3**); drug treatment or placebo was given for up to 24 or 28 days respectively, prior to resection of tumor.

In a previous phase I dose escalation study of heavily-pretreated patients with either CLL or non-Hodgkin lymphoma, AMG319 doses of up to 400mg were explored without reaching a maximally-tolerated dose, and exhibited PK dynamics with a mean half-life of 3.8-6.6h in plasma[25]. In that phase 1 study, daily dosing with 400mg AMG319 led to near complete target inhibition (BCR-induced pAKT in *ex vivo* IgD-stimulated CLL samples) and >50% nodal regression[25], while immune related adverse events (irAE) at grade 3 or above according to the common toxicity criteria (CTC) occurred after days 40 and 60. We thus reasoned that high grade irAEs were unlikely to occur during the shorter treatment duration in the neoadjuvant setting (**Extended Data Fig.3a),** and therefore selected 400 mg/day as the starting dose.

The intended time from initiating treatment with AMG319 or placebo to surgical resection of tumor was up to 4 weeks, with weekly blood draws. Thirty-three patients were randomized in a 2:1 ratio (AMG319:Placebo) to the trial and 30 patients received at least one dose of AMG319 or placebo. Fifteen patients received 400 mg daily of AMG319 (range of 7–24 days per patient). Unexpectedly, at the 400 mg dose, 9/15 patients experienced irAEs that lead to withdrawal of treatment (**Extended Data Table 3**). After a formal safety review, 6 additional patients were recruited and treated at a reduced dose of 300 mg per day. Again, 3/6 patients had irAEs that led to discontinuation of treatment (**Extended Data Table 3**) although the planned sample size of 54 randomized patients had not been reached. One patient experienced grade 4 colitis after completion of 24 daily doses of AMG319, and eventually required colectomy; the study was discontinued at this point. Overall, 9 patients were randomized to the placebo arm (**Extended Data Fig. 3a**), of these, one experienced a serious adverse event (grade 4 post-surgical infection). We measured target inhibition (pAKT levels in B cells; **Fig. 3b**) and drug levels (**Fig. 3c**) to verify drug administration (**Extended Data Table 3**). Pharmacokinetic (PK) analysis indicated peaking drug levels on day 8; 8/10 patients who discontinued treatment did so between day 7 and 9 (**Extended Data Table 3**), which resulted in loss of detectable drug in the PK analysis on day 15 (**Fig. 3c**). As expected,

AMG319 treatment caused a significant decrease in the pAKT levels in B cells[1] 4h post-treatment on day 1 and day 15 (**Fig. 3b** and **Extended Data Table 3**). Interestingly, modulation of PI3Kδ did not appear to affect humoral IgG responses to vaccination with the recall antigen tetanus toxoid (**Fig. 3d**), while we observed few tetanus-specific T cells in either the AMG319 or placebo treated patients (**Extended Data Table 3**), pointing to an overall degree of functional immunocompromise in our patient cohort.

Clinically, and most likely reflecting the brief treatment period, we did not observe any significant differences in the measured tumor volumes between the study arms in the 23 patients in whom this was evaluable. Two partial responses (PR) and one pathological complete response occurred in AMG319-treated patients (**Extended Data Fig. 3b**); one PR was observed in the control group. The full evaluation of radiological measurements has previously been reported at https://www.clinicaltrialsregister.eu/ctr-search/trial/2014-004388-20/results to the EU Clinical Trials Register in compliance with regulatory requirements.

**PI3Kδ inhibition displaces activated $T_{REG}$ cells into circulation**

To investigate whether PI3Kδi, akin to our findings in preclinical models (**Fig. 2 and Extended Data Fig.2**), affects tissue-residency and functionality of $T_{REG}$ cells, we assessed the frequency and phenotype of circulating $T_{REG}$ cells over the course of the treatment. We observed a significant treatment-related increase in the percentage of circulating $T_{REG}$ cells ($CD4^+CD25^+CD127^{lo}$) (**Fig. 4a**), while the proportion of $T_{REG}$ cells in the placebo group remained stable (**Extended Data Fig. 3c**). In addition, we observed a significant increase in the expression levels of ICOS[42], PD-1[43], GITR[44] and 4-1BB[45], markers of cell activation and recent antigen encounter, in circulating $T_{REG}$ cells (**Fig. 4b**). Together, these data indicate that PI3Kδi treatment can displace activated $T_{REG}$ cells from tissues, including tumor tissues, into the circulation, presumably by altering the expression of tissue homing factors like KLF2 and S1PR1, direct targets of FOXO1. In line with these findings, we also observed frequent, and in a few patients, severe grade 3/4 irAEs in the AMG319-treated patients (**Extended Data Table 3**). Of the 91 total irAEs we observed, 85 were in the AMG319 treatment group and 6

in the placebo group; all 23 grade 3 and 1 grade 4 irAEs could be attributed to AMG319 treatment (**Fig. 4c**). The most prevalent irAEs were skin rashes (29%; 25% observed in the treatment group and 4% in placebo group), diarrhea (29%; 28% in observed treatment group and 1% in placebo group) and transaminitis (14% all of which were observed in the treatment group), consistent with a loss of $T_{REG}$ cells or $T_{REG}$ cell functionality in multiple tissues causing immunopathology (**Fig. 2c** and **Extended Data Table 3**). Unlike the phase 1 dose-escalation study of AMG319 in heavily pretreated patients with either CLL or non-Hodgkin lymphoma[25], the onset of irAEs was surprisingly rapid and led to treatment discontinuation in 12/21 AMG319-treated patients.

**Intratumoral $CD8^+$ T cells exhibit signs of heightened cytotoxic potential**

To assess the impact of PI3Kδi treatment on anti-tumor immune responses, we first performed bulk RNA-seq in pre- and post-treatment tumor samples. Differential gene expression analysis revealed substantial differences in the AMG319-treatment group (93 differentially-expressed genes (DEGs)), but not for the placebo group (3 DEGs) (**Fig. 5a, b** and **Extended Data Table 4**). PI3Kδ-inhibition disrupted expression of genes in the PI3K pathway, as assessed by gene set enrichment analysis (GSEA) (**Extended Data Fig. 4a**), and led to a significant reduction in *FOXP3* transcript levels in the tumor samples (**Fig. 5b, Extended Data Fig. 4b**). While immunohistochemistry analysis (IHC) showed a similar trend towards fewer $T_{REG}$ cells (**Extended Data Fig. 4c** and **Extended Data Table 3**), this did not reach statistical significance in the pairwise evaluation, likely because small pre-treatment biopsies precluded accurate cell counts. Interestingly, gene ontology pathway analyses of the DEGs in AMG319 pre- and post-treatment samples showed a significant overlap with genes involved in angiogenesis-related pathways (**Extended Data Fig. 4d** and **Extended Data Table 4**). The significant downregulation of angiogenesis and vascular development-related genes suggests a potential of PI3Kδ inhibition to reduce neovascularization in tumors and thus curb tumor growth, potentially mediated by the depletion of intratumoral $T_{REG}$ cells, which has been shown to promote angiogenesis[46]. In the AMG319-treatment group, we also found

significantly higher expression of *GZMA*, and a trend (p=0.06) towards higher expression of *PRF1* (encoding for Perforin-1) in post-treatment tumor samples (**Extended Data Fig. 4e,f**), implying an increase in the number or activity of cytotoxic cells. We corroborated these results with bulk-RNA-seq analysis of sorted tumor-infiltrating $CD8^+$ T cells from 2 patients in whom paired tumor samples were available pre and post PI3Kδi treatment (**Fig. 5c**). We found higher expression of *IFNG, GZMB and PRF1* in post-treatment samples, which indicated enhanced cytotoxic potential of tumor-infiltrating $CD8^+$ T cells following PI3Kδi treatment, consistent with our murine data (**Fig. 1e)**.

To contextualize our data, we compared expression levels of *CD8A* as a measure of TIL infiltration with data from a previous HNSCC patient cohort (**Extended data table 4**)[40]. Our analysis revealed low baseline TIL infiltration in the majority of the samples in our trial (**Fig. 5d**), consistent with the notion that HPV-negative cancers are predominantly immune-cold tumors. These data, as well as the intermittent dosing of AMG319 in a neoadjuvant setting, also contribute to our understanding as to why a primary efficacy endpoint of the study, a doubling in $CD8^+$ TILs assessed by IHC, was not met. AMG-319 nonetheless further reduced the $T_{REG}$ cell frequency in these tumors (**Extended Data Fig. 4b,c)** and increased expression of markers associated with cytotoxic function, consistent with our murine data (**Fig. 1e)**.

**PI3Kδ inhibition drives oligoclonal T cell expansion**

To assess the consequences of PI3Kδ-inhibition on anti-tumor immunity in more detail, we next performed combined single-cell RNA-seq and TCR-seq analysis of tumor-infiltrating $CD3^+$ T cells from 6 patients with available pre-and post-treatment tumor samples. UMAP analysis demonstrated separation of $CD4^+$ from $CD8^+$ T cells (**Fig. 6a**). Single-cell differential gene expression analysis of the $CD4^+$ and $CD8^+$ clusters showed a treatment-related increase in expression of cytotoxicity genes (*e.g. GZMB* and *PRF1*) (**Extended Data Table 5**, **Fig. 5b**), in line with our previous results (**Fig. 1e** and **Fig. 5c**) and implying that tumor-infiltrating $CD4^+$ and $CD8^+$ T cells exhibit enhanced cytotoxic properties following PI3Kδi treatment.

Accordingly, Ingenuity Pathway Analysis (IPA) of the differentially-expressed genes in $CD8^+$ T cells identified CSF2 (GM-CSF), a pro-inflammatory mediator and indicator of tissue inflammation that can enhance the generation of CTLs[47,48], IL-2 and TCR as the top 3 upstream regulators (**Extended Data Table 6**), indicative of pro-survival IL-2 signalling and TCR activation. Crucially, and in line with these findings, our single-cell TCR-seq data demonstrate substantial clonal expansion of $CD8^+$ T cells, and to a lesser degree of $CD4^+$ T cells, post-treatment (**Fig. 6c,d**). Several, but not all, of these clonally-expanded $CD8^+$ T cells were also present in pre-treatment samples, suggesting that PI3Kδ inhibition drives the expansion of both new and pre-existing T cells. Together, these data indicate that PI3Kδ inhibition causes profound changes in the TME, characterized by enhanced $CD4^+$ and $CD8^+$ T cell activation, oligoclonal T cell expansion and increased cytolytic activity, consistent with a decrease in intratumoral $T_{REG}$ cells, ensuing T cell activation.

**Discussion**

PI3K inhibitors were initially considered to mainly target cancer cell-intrinsic PI3K activity, which was the underlying rationale to test inhibitors against the leukocyte-enriched PI3Kδ in hematological malignancies. However, subsequent studies have shown that PI3Kδ inhibition also has clear immunomodulatory activities, largely T-cell mediated, which were under-appreciated at the time of the early trials in B-cell malignancies, causing irAEs that have hampered clinical progress and utility. Several lines of evidence suggest that PI3Kδi preferentially inhibit $T_{REG}$ cells over other T cell subsets[8,9,11,12,14] but to date, no trials have been performed to explicitly explore this concept in humans. Our current study provides the first in-depth investigation on the immune impact of PI3Kδ inhibition in patients with solid tumors.

We find that in the tumor tissue, PI3Kδ inhibition leads to substantial changes in the cell composition of the TME by reducing $T_{REG}$ cells and activating intratumoral $CD4^+$ and $CD8^+$ T cells, which clonally expand and display heightened cytotoxic and cytolytic features. However, in the circulation, paradoxically, we found increased number of $T_{REG}$ cells. Because

these $T_{REG}$ cells expressed higher levels of ICOS[42], PD-1[43], GITR[44] and 4-1BB[45], markers indicating recent cell activation following antigen encounter, we hypothesize that PI3Kδ inhibition may displace activated tissue $T_{REG}$ cells into the circulation and leave the normal tissues vulnerable to inflammation, presumably triggered by the unrestrained activity of effector T cells. These observations are consistent with previous studies, implying that alterations of the PI3Kδ-Foxo1 pathway affect the trafficking of $T_{REG}$ cells by altering the expression of lymphoid homing molecules[7]. In support of this hypothesis, we find that PI3Kδ inhibition in mice causes systemic changes in the $T_{REG}$ cell compartment and differentially affects $T_{REG}$ subsets in different organ systems. Notably, we find substantial changes in the transcriptional features and composition of colonic $T_{REG}$ cell subsets, which indicate that PI3Kδ inhibition impacts $T_{REG}$ functionality, survival and tissue retention, thus altering $T_{REG}$ cell frequencies or $T_{REG}$ subtype compositions in both tumor and non-malignant tissues. Overall, our complementary studies in mice and humans highlight potential mechanisms that drive irAEs and anti-tumor activity of PI3Kδi.

Compared to the heavily-pretreated patients in the AMG319 trial in B-cell malignancies (number of prior treatment regimens ranging from 1-9 for CLL and 5-9 for NHL)[25], treatment-naïve patients with operable, untreated HNSCC, appeared to be much more sensitive to PI3Kδ-inhibition, both in terms of the frequency of irAEs and the onset of these events after a short treatment period. Our data show that the immunomodulatory effects of PI3Kδi need to be evaluated judiciously in treatment-naïve patients, unaffected by multiple lines of treatment and the immunosuppressive effect of hematological malignancies such as CLL. It is clear that in the neoadjuvant setting in patients with HNSCC, at the evaluated doses and with daily scheduling, PI3Kδ inhibition exhibits an unfavorable safety profile, limiting its feasibility and clinical benefit by causing frequent and severe grade 3/4 irAEs, most likely driven by modulation of $T_{REG}$ cell behaviour in non-malignant tissues. In the context of B-cell malignancies, studies adapting PI3Kδi dosing and scheduling regimens have shown promising results which might also facilitate combination therapies. Decreased dosages and an altered PI3Kδi treatment regimen will also be required in solid tumors, especially in immune

competent patients, in order to be able to exploit the clear anti-tumor immune response induced by PI3Kδi while limiting the adverse effects associated with reduced $T_{REG}$ function in healthy tissues. Finally, our data suggest that the unique cellular composition of stimulatory *versus* regulatory cells in the TME of each patient might be an important determinant of the efficacy of PI3Kδ inhibition. As such, PI3Kδi might be especially useful in patients with high levels of intratumoral $T_{REG}$ cells and an unfavorable ratio of $T_{REG}$ versus $CD8^+$ TILs in pre-treatment samples. Hence, our study sets the stage for further exploration of PI3Kδi as immunomodulatory agents in solid tumors.

**Acknowledgements:**

We thank Christian Rommel, Khaled Ali, Peter Johnson and David Scott for support and help during the initial phases of setting up the CRUK/Amgen collaboration. We thank Maria Lopez and the research pathology core at University Hospital Southampton for performing the immunohistochemistry on the paraffin embedded material, Isla Henderson for help with the tetanus ELISAs, the La Jolla Institute (LJI) Flow Cytometry Core for assisting with cell sorting, the LJI sequencing core for the bulk and single cell sequencing and Dr. Gary Means, Amgen for method and training for the phospho-AKT assays. We thank emeritus Professor Peter Friedmann for constructive critique of the paper and Dr. Divya Singh for advice on experimental work. This work was funded by a CDD trial Grant CRUKD/15/004, a Cancer Research UK Centres Network Accelerator Award Grant (A21998), O.W., K.MC and J.T.), the CRUK and NIHR Experimental Cancer Medicine Center (ECMC) Southampton (A15581), the CRUK and NIHR ECMC Liverpool (A25153), Cancer Research UK Programme Grant (C23338/A25722, E.L-G and B.V.); the UK NIHR UCLH Biomedical Research Centre (B.V.), S10OD025052 (Illumina Novaseq6000), the William K. Bowes Jr Foundation (P.V.), and Whittaker foundation (P.V., LC, C.H.O.) the Deutsche Forschungsgemeinschaft DFG research fellowship # WI 5255/1-1:1 (AvW). The clinical delivery of this work was supported by the Wessex Clinical Research Network and National Institute of Health Research UK. We further acknowledge Cancer Research UK (Centre for Drug Development) as the clinical trial

Sponsor and for funding and management of the Phase II clinical trial, as well as Amgen for supply of the PI3Kδi AMG319.

**Author contribution and acknowledgements**

SE: study design, experimental work, data interpretation, paper writing;
CR-S: bioinformatic evaluation, data interpretation, paper review;
EK: study design, patient recruitment, paper review;
LC: data collation, data interpretation, paper writing and review;
JT: bioinformatic evaluation, data interpretation, paper review;
OW: experimental work, data interpretation, paper review;
AvW: experimental work, data interpretation, paper review;
DJ: experimental work, data interpretation, paper review;
KMC: experimental work, data interpretation, paper review;
HS, MM, AW: experimental work, paper review;
EL-G: experimental work, provision of study materials, data interpretation, paper review
YL: experimental work, paper review;
NAD, LE, FK: study conduct, safety data review, and monitoring, data review and verification for sponsor
GA: study design, safety review, data review
GH: generation and provision of placebo and IMP
JJS, AGS, RS, JAMC, CP, JHD, PB, RPS: patient recruitment, paper review
PL: data generation and interpretation, paper review
WW: study design, statistical review for sponsor
AH: study design, statistical review
GJT: histopathological evaluation, data generation and interpretation, paper review
TMJ: study development, patient recruitment, paper review
FA, bioinformatic analyses and supervision, data review, paper review
KO: study design, paper writing and review
BV: study design, paper writing and review
*PV: study design, data generation and review, paper writing and review.
*&CHO: study design, patient recruitment, data generation and review, paper writing and review.
*PV and CHO conceived, supervised and led the work
&Corresponding author

**References**


1. Lucas, C. L., Chandra, A., Nejentsev, S., Condliffe, A. M. & Okkenhaug, K. PI3Kδ and primary immunodeficiencies. *Nat. Rev. Immunol.* **16**, 702–714 (2016).
2. Furman, R. R. *et al.* Idelalisib and Rituximab in Relapsed Chronic Lymphocytic Leukemia. *N. Engl. J. Med.* (2014) doi:10.1056/nejmoa1315226.
3. Gopal, A. K. *et al.* PI3Kδ Inhibition by Idelalisib in Patients with Relapsed Indolent Lymphoma. *N. Engl. J. Med.* (2014) doi:10.1056/nejmoa1314583.
4. Vanhaesebroeck, B. PI3K inhibitors are finally coming of age. *Nat. Rev. Drug Dev.* Accepted for publication, (2021).
5. Patton, D. T. *et al.* Cutting Edge: The Phosphoinositide 3-Kinase p110δ Is Critical for the Function of CD4 + CD25 + Foxp3 + Regulatory T Cells . *J. Immunol.* (2006) doi:10.4049/jimmunol.177.10.6598.
6. Okkenhaug, K. *et al.* The p110δ Isoform of Phosphoinositide 3-Kinase Controls Clonal Expansion and Differentiation of Th Cells. *J. Immunol.* (2006) doi:10.4049/jimmunol.177.8.5122.
7. Luo, C. T., Liao, W., Dadi, S., Toure, A. & Li, M. O. Graded Foxo1 activity in Treg cells differentiates tumour immunity from spontaneous autoimmunity. *Nature* **529**, 532–536 (2016).
8. Ali, K. *et al.* Inactivation of PI(3)K p110δ breaks regulatory T-cell-mediated immune tolerance to cancer. *Nature* **510**, 407–411 (2014).
9. Lim, E. L. *et al.* Phosphoinositide 3-kinase δ inhibition promotes antitumor responses but antagonizes checkpoint inhibitors. *JCI insight* (2018) doi:10.1172/jci.insight.120626.
10. Abu-Eid, R. *et al.* Selective inhibition of regulatory T cells by targeting the PI3K-Akt pathway. *Cancer Immunol. Res.* (2014) doi:10.1158/2326-6066.CIR-14-0095.
11. Chellappa, S. *et al.* The PI3K p110δ Isoform Inhibitor Idelalisib Preferentially Inhibits Human Regulatory T Cell Function. *J. Immunol.* (2019) doi:10.4049/jimmunol.1701703.
12. Lampson, B. L. *et al.* Idelalisib given front-line for treatment of chronic lymphocytic leukemia causes frequent immune-mediated hepatotoxicity. *Blood* (2016) doi:10.1182/blood-2016-03-707133.
13. Lampson, B. L. & Brown, J. R. PI3Kδ-selective and PI3Kα/δ-combinatorial inhibitors in clinical development for B-cell non-Hodgkin lymphoma. *Expert Opinion on Investigational Drugs* (2017) doi:10.1080/13543784.2017.1384815.
14. Lim, E. L. & Okkenhaug, K. Phosphoinositide 3-kinase δ is a regulatory T-cell target in cancer immunotherapy. *Immunology* (2019) doi:10.1111/imm.13082.
15. Pompura, S. L. & Dominguez-Villar, M. The PI3K/AKT signaling pathway in regulatory

T-cell development, stability, and function. *J. Leukoc. Biol.* **103**, 1065–1076 (2018).
16. Huynh, A. *et al.* Control of PI(3) kinase in Tregcells maintains homeostasis and lineage stability. *Nat. Immunol.* **16**, 188–196 (2015).
17. Gerriets, V. A. *et al.* Foxp3 and Toll-like receptor signaling balance T reg cell anabolic metabolism for suppression. *Nat. Immunol.* (2016) doi:10.1038/ni.3577.
18. Tan, C. L. *et al.* PD-1 restraint of regulatory T cell suppressive activity is critical for immune tolerance. **218**, (2020).
19. Dong, S. *et al.* PI3K p110δ inactivation antagonizes chronic lymphocytic leukemia and reverses T cell immune suppression. *J. Clin. Invest.* (2019) doi:10.1172/JCI99386.
20. Abu Eid, R. *et al.* Enhanced therapeutic efficacy and memory of tumor-specific CD8 T cells by ex vivo PI3K-δ inhibition. *Cancer Res.* (2017) doi:10.1158/0008-5472.CAN-16-1925.
21. Ahmad, S. *et al.* Differential PI3Kδ signaling in CD4+ T-cell subsets enables selective targeting of t regulatory cells to enhance cancer immunotherapy. *Cancer Res.* (2017) doi:10.1158/0008-5472.CAN-16-1839.
22. Lu, X. *et al.* Effective combinatorial immunotherapy for castration-resistant prostate cancer. *Nature* (2017) doi:10.1038/nature21676.
23. Lauder, S. N. *et al.* Enhanced antitumor immunity through sequential targeting of PI3Kδand LAG3. *J. Immunother. Cancer* (2020) doi:10.1136/jitc-2020-000693.
24. Gyori, D. *et al.* Compensation between CSF1R+ macrophages and Foxp3+ Treg cells drives resistance to tumor immunotherapy. *JCI insight* (2018) doi:10.1172/jci.insight.120631.
25. Lanasa, M. C. *et al.* First-In-Human Study Of AMG 319, a Highly Selective, Small Molecule Inhibitor Of PI3Kδ, In Adult Patients With Relapsed Or Refractory Lymphoid Malignancies. *Blood* (2013) doi:10.1182/blood.v122.21.678.678.
26. Scott, A. C. *et al.* TOX is a critical regulator of tumour-specific T cell differentiation. *Nature* (2019) doi:10.1038/s41586-019-1324-y.
27. Khan, O. *et al.* TOX transcriptionally and epigenetically programs CD8+ T cell exhaustion. *Nature* (2019) doi:10.1038/s41586-019-1325-x.
28. Alfei, F. *et al.* TOX reinforces the phenotype and longevity of exhausted T cells in chronic viral infection. *Nature* (2019) doi:10.1038/s41586-019-1326-9.
29. DiSpirito, J. R. *et al.* Molecular diversification of regulatory T cells in nonlymphoid tissues. *Sci. Immunol.* **3**, eaat5861 (2018).
30. Miragaia, R. J. *et al.* Single-Cell Transcriptomics of Regulatory T Cells Reveals Trajectories of Tissue Adaptation. *Immunity* (2019) doi:10.1016/j.immuni.2019.01.001.
31. Wing, J. B., Ise, W., Kurosaki, T. & Sakaguchi, S. Regulatory T cells control antigen-specific expansion of Tfh cell number and humoral immune responses via the

coreceptor CTLA-4. *Immunity* **41**, 1013–1025 (2014).

32. Ovcinnikovs, V. *et al.* CTLA-4-mediated transendocytosis of costimulatory molecules primarily targets migratory dendritic cells. *Sci. Immunol.* **4**, (2019).
33. Zhang, N. *et al.* Regulatory T Cells Sequentially Migrate from Inflamed Tissues to Draining Lymph Nodes to Suppress the Alloimmune Response. *Immunity* (2009) doi:10.1016/j.immuni.2008.12.022.
34. Delacher, M. *et al.* Precursors for Nonlymphoid-Tissue Treg Cells Reside in Secondary Lymphoid Organs and Are Programmed by the Transcription Factor BATF. *Immunity* (2020) doi:10.1016/j.immuni.2019.12.002.
35. Whibley, N., Tucci, A. & Powrie, F. Regulatory T cell adaptation in the intestine and skin. *Nature Immunology* (2019) doi:10.1038/s41590-019-0351-z.
36. Arpaia, N. *et al.* A Distinct Function of Regulatory T Cells in Tissue Protection. *Cell* (2015) doi:10.1016/j.cell.2015.08.021.
37. Aaronson, D. S. & Horvath, C. M. A road map for those who don't know JAK-STAT. *Science* (2002) doi:10.1126/science.1071545.
38. Hu, X. & Ivashkiv, L. B. Cross-regulation of Signaling Pathways by Interferon-γ: Implications for Immune Responses and Autoimmune Diseases. *Immunity* (2009) doi:10.1016/j.immuni.2009.09.002.
39. Ward, M. J. *et al.* Staging and treatment of oropharyngeal cancer in the human papillomavirus era. *Head Neck* (2015) doi:10.1002/hed.23697.
40. Wood, O. *et al.* Gene expression analysis of TIL rich HPV-driven head and neck tumors reveals a distinct B-cell signature when compared to HPV independent tumors. *Oncotarget* **7**, 56781–56797 (2016).
41. Ottensmeier, C. H. *et al.* Upregulated Glucose Metabolism Correlates Inversely with CD8 $^{+}$ T-cell Infiltration and Survival in Squamous Cell Carcinoma. *Cancer Res.* **76**, 4136–4148 (2016).
42. Dong, C. *et al.* ICOS co-stimulatory receptor is essential for T-cell activation and function. *Nature* (2001) doi:10.1038/35051100.
43. Oestreich, K. J., Yoon, H., Ahmed, R. & Boss, J. M. NFATc1 Regulates PD-1 Expression upon T Cell Activation. *J. Immunol.* (2008) doi:10.4049/jimmunol.181.7.4832.
44. Shimizu, J., Yamazaki, S., Takahashi, T., Ishida, Y. & Sakaguchi, S. Stimulation of CD25+CD4+ regulatory T cells through GITR breaks immunological self-tolerance. *Nat. Immunol.* (2002) doi:10.1038/ni759.
45. Kniemeyer, O., Brakhage, A. A., Ferreira, F., Wallner, M. & Sawitzki, B. Regulatory T Cell Specificity Directs Tolerance versus Allergy against Aeroantigens in Humans. *Cell* **167**, 1067-1078.e16 (2016).

46. Wang, H., Franco, F. & Ho, P. C. Metabolic Regulation of Tregs in Cancer: Opportunities for Immunotherapy. *Trends in Cancer* **3**, 583–592 (2017).
47. Becher, B., Tugues, S. & Greter, M. GM-CSF: From Growth Factor to Central Mediator of Tissue Inflammation. *Immunity* (2016) doi:10.1016/j.immuni.2016.10.026.
48. Jäger, E. *et al.* Granulocyte-macrophage-colony-stimulating factor enhances immune responses to melanoma-associated peptides in vivo. *Int. J. Cancer* **67**, 54–62 (1996).
49. Juneja, V. R. *et al.* PD-L1 on tumor cells is sufficient for immune evasion in immunogenic tumors and inhibits CD8 T cell cytotoxicity. *J. Exp. Med.* **214**, 895–904 (2017).
50. Vijayanand, P. *et al.* Invariant Natural Killer T Cells in Asthma and Chronic Obstructive Pulmonary Disease. *N. Engl. J. Med.* (2007) doi:10.1056/nejmoa064691.
51. Patil, V. S. *et al.* Precursors of human CD4 + cytotoxic T lymphocytes identified by single-cell transcriptome analysis. *Sci. Immunol.* **3**, 8664 (2018).
52. Finak, G. *et al.* MAST: A flexible statistical framework for assessing transcriptional changes and characterizing heterogeneity in single-cell RNA sequencing data. *Genome Biol.* **16**, 278 (2015).

**Figure 1: PI3Kδ-inhibition induces are pro-inflammatory tumor microenvironment**

**a**, Mice were inoculated *s.c.* with B16F10-OVA cells and fed either a control diet or a diet containing the PI-3065 PI3Kδ inhibitor for the indicated treatment period. Tumor volume (**a**) and flow-cytometric analyses of cell frequencies (**b-g**) of mice treated as indicated. **h**, Shown are representative contour plots of intratumoral $CD8^+$ T cells depicting the indicated markers. n=9-10 mice/group. Data are mean +/- S.E.M. Significance for comparisons were computed using Mann-Whitney test are the data are representative of two independent experiments.

**Figure 2: PI3Kδ inhibition affects distinct $T_{REG}$ cell subtypes**

**a-c**, Analysis of 10x single-cell RNA-seq data displayed by UMAP analysis. Seurat clustering of $FoxP3^+CD4^+$ T cells independent of treatment (**a**), in placebo-treated control mice (**b**) and PI-3065-treated mice (**c**). **d-f**, Volcano plots of single-cell RNA-seq analysis of placebo-treated control mice and PI-3065-treated mice in spleen (**d**) tumor (**e**) and colon (**f**). Highlighted are transcripts with a >0.5 log2 fold change. **g**, Curtain plot highlighting selected genes in each cluster with average transcript expression (color scale) and percent of expressing cells (size scale). **h**, Violin plots showing normalized expression levels ($log_2$(CPM+1)) of highlighted genes in cluster 0 and cluster 8

**Figure 3: AMG319 causes significant immune related adverse events**

**a**, Trial schematic of the placebo-controlled dose escalation study. **b**, Assessment of the level of AKT phosphorylation in B cells at indicated time points pre-dose and 4h after treatment with AMG319, data from one representative patient are shown. **c**, Plasma concentrations of AMG319 in placebo-controlled and drug-treated patients at indicated time points. Highlighted in red are patients who were either on-treatment or had only recently (2 days prior to analysis) or briefly discontinued treatment. **d**, Evaluation of the humoral immune response to tetanus vaccination (day 8) using ELISA.

**Figure 4: AMG319 displaces activated $T_{REG}$ cells into circulation**

**a,b**, Representative contour plots of $CD3^+$ T cells and $T_{REG}$ cells and flow-cytometric analyses of the frequency of (**a**) and expression of activation markers (**b**) in circulating $T_{REG}$ cells in AMG319-treated patients at indicated time points. **c**, Frequency, type and severity of observed immune related adverse events in placebo and AMG319-treated patients. Data are mean +/- S.E.M. Significance for comparisons were computed using Wilcoxon matched-pairs signed rank test (**a,b**).

**Figure 5: AMG319 treatment changes the cellular composition of the tumor microenvironment**

**a-c** Volcano plots of whole tumor RNA-seq analysis (**a,b**) or bulk RNA-seq analysis of $CD8^+$ T cells (**c**) comparing AMG-319 to placebo treated patients. Differentially expressed genes between pre and post-treatment samples are highlighted in red. Depicted are transcripts that change in expression more than 0.75-fold and adjusted *P* value of ≤ 0.1 (**a,b**) or <0.05 (**c**). **d**, Stratification into TIL status (TIL lo, TIL mod, and TIL hi) from samples of patients enrolled in this study in comparison to a previously published HNSCC cohort.

**Figure 6: Single-cell RNA-seq analysis reveals substantial oligoclonal expansion of tumor-infiltrating $CD8^+$ T cells post-treatment**

**a**, Analysis of smart-seq2 single-cell RNA-seq data of sorted tumor-infiltrating $CD3^+$ T cells displayed by UMAP analysis. **b**, Violin plots depicting the expression of differentially expression highlighted genes in $CD4^+$ T cells (left) or $CD8^+$ T cells (right). **c**, TraCer plots of all clonally expanded $CD4^+$ and $CD8^+$ T cells (=/>2 clonotypes) in pre- and post-treatment samples of AMG319-treated patients. **d**, Percentages of non-expanded and expanded $CD8^+$ and $CD4^+$ T cell clones in pre- *versus* post-treatment samples.

**Extended Data Figure 1: PI3Kδ inhibition enhances anti-tumor immunity**

**a**, Mice were inoculated *s.c.* with B16F10-OVA cells and fed a control diet or a diet containing the PI3Kδ inhibitor PI-3065 over the indicated treatment period. Tumor volume (**a**) and flow-cytometric analyses of $T_{REG}$ cell frequencies (**b**) in indicated organs of mice treated as indicated, n=5-6 mice/group. Shown are representative contour plots of FoxP3-expressing ($RFP^+$) $CD4^+$ T cells in indicated organs. Data are mean +/- S.E.M., Significance for comparisons were computed using Mann-Whitney test are the data are representative of two independent experiments.

**Extended Data Figure 2: $T_{REG}$ cells in different tissues exhibit unique transcriptomic signatures**

**a**, Analysis of 10x single-cell RNA-seq data displayed by UMAP analysis. Seurat clustering of $FoxP3^+CD4^+$ T cells in spleen (left), tumor (middle) and colon (right). **b**, Heatmap comparing gene expression of cells in all clusters. Depicted are transcripts that change in expression more than 0.5-fold and adjusted *P*value of ≤ 0.05. **c**, Bar charts depicting the proportion of cells in each cluster colorized based on cells in indicated treatments making up the cluster. **d**, Violin plots showing normalized expression levels ($log_2$(CPM+1)) of highlighted genes in cluster the colonic clusters. **e-h**, Flow-cytometric analyses of $CD8^+$ T cell frequencies in colon (**e**), spleen (**f**) and of the expression of PD-1 (**g**) and ICOS (**h**) on colonic $CD8^+$ T cells, n=5-7 mice/group. Data in **e-h** are mean +/- S.E.M. Significance for comparisons were computed using Mann-Whitney test are the data are representative of two independent experiments.

**Extended Data Figure 3: Trial schematic**

**a**, 36 patients were screened, of which 33 were recruited and randomly allocated to the placebo control arm or AMG319 drug-treatment arm; 30 patients ultimately received at least one dose of either AMG319 or placebo. Of the 21 patients that were treated with AMG319, 6 patients received daily doses of 300 mg and 15 patients (2 patients withdrew consent prior to receiving the first dose) received daily doses of 400 mg. An initial biopsy was taken before

trial initiation and surgical resection of tumors was performed 4-6 weeks after the first dose of treatment. Pre- on- and post-treatment blood samples were collected for further analysis. **b**, Waterfall plot depicting the change in tumor volume from screening to pre-surgery measured by MRI scan in patients treated with AMG319 (yellow bars) or placebo (green bars), shown are all patients for which MRI scans have been performed **c**, Flow-cytometric analyses of the frequency of and expression of activation markers in circulating $T_{REG}$ cells in placebo-treated patients at indicated time points.

**Extended Data Figure 4: Low levels of TIL infiltration in most AMG319-treated patients**

**a,** Gene set enrichment analysis for genes in the PI3K:AKT network of differentially-expressed transcripts (n=93) of the whole tumor RNA-seq of AMG319-treated patients (**Fig. 4b**). **b**,**c**,**e,f** Expression levels (TPM) (**b,e,f**) and IHC analysis (**c**) showing proportion of $FOXP3^+$ cells in pre- and post-treatment samples of placebo- or AMG319-treated patients. **d**, Gene ontology pathway analysis of differentially-expressed transcripts (n=93) in **Fig. 4b**. Significance for comparisons were computed using Wilcoxon matched-pairs signed rank test.

## Methods

### Mice

C57BL/6J mice were obtained from the Jackson labs. FoxP3$^{RFP}$ mice were a gift from Stephen Schoenberger (La Jolla Institute for Immunology). All mice were between 6-12-week-old at the beginning of the experiment;. the animal work was approved by the relevant La Jolla institute for Immunology Animal Ethics Committee. B16F10-OVA cells were a gift from Prof. Linden (La Jolla Institute for Immunology). Cell lines tested negative for mycoplasma infection and were treated with Plasmocin to prevent contamination.

### Tumor experiments

Mice were inoculated with 1-1.5x$10^5$ B16F10-OVA cells subcutaneously into the right flank. Mice were put on either a control diet or a diet containing a PI3Kδ inhibitor PI-3065 on day 1 or day 5 after tumor inoculation. Diets were prepared using powdered 2018 global rodent diet (Envigo) mixed with or without PI-3065 at 0.5 g/kg, which corresponds to a daily dose of 75 mg/kg as used in our previous study[2]. To pellet the food, 50% v/w water was added to the diet and dough thoroughly mixed, compressed, moulded and dried before use. Tumor size was monitored every other day, and tumor harvested at indicated time points for analysis of tumor-infiltrating lymphocytes. Tumor volume was calculated as ½ x D x $d^2$, where D is the major axis and d is the minor axis, as described previously[49].

### Double blind, randomised clinical trial and sample collection

The study was sponsored by Cancer Research UK Center for Drug Development (CRUKD/15/004) and approved by the Southampton and South West Hampshire Research Ethics Board; the trial EudraCT number is 2014-004388-20. Detailed information about the trial design, randomization procedure, protocol amendments, recruitment data, patient characteristics and adverse events are deposited at https://www.clinicaltrialsregister.eu/ctr-search/trial/2014-004388-20/results#moreInformationSection. Primary endpoints were safety and assessment of $CD8^+$ immune infiltrates, secondary endpoints tumor responses and AMG319 pharmacokinetic evaluation (https://www.clinicaltrialsregister.eu/ctr-

search/trial/2014-004388-20/results#endPointsSection). The sample size has been calculated as follows: in a pilot cohort, the CD8 count in the biopsy taken at diagnosis, and in the resected tissue sample was quantified. The mean value at diagnosis was 25 cells/high power filed (hpf), and this remained almost the same in the resected sample (26 cells). With an observed standard deviation of five cells we posited we would observe a doubling to 50 cells/hpf following treatment with AMG 319, hence a difference between the two treatment groups of 25. To detect a standardised difference of 0.5 with 80% power and one-sided test of statistical significance of 20%, we required 36 patients to be randomised to AMG 319 and 18 to placebo (54 in total). Randomisation was at the level of the individual patient, using block randomisation with randomly varying block sizes. During the course of the clinical trial the randomisation list was held by the unblinded Trial Statistician and within the IWRS. Patients and care providers were blinded to the treatment allocation, and all immunological evaluations were completed by a pathologist and researchers who were blinded to the patient allocation to treatment arms. Patients were recruited from October 2015 to May 2018 at in the UK (University Hospital Southampton NHS Foundation Trust, Poole Hospitals NHS Foundation Trust, Liverpool University Hospitals NHS Foundation Trust and Queen Elizabeth University Hospital Glasgow, two additional centers did not recruit patients); written informed consent was obtained from all subjects. Patients were eligible if they were ≥18 years, with histologically proven HNSCC for whom surgery was the primary treatment option, with laboratory results within specified ranges. Patients had to be clinically eligible for tumor resection; patients who had undergone prior radio/immuno/chemotherapy or other anti-cancer therapy for their current HNSCC, were excluded. Clinical data were obtained for age, gender, tumour size (T stage), and nodal status (N stage) (summarised in Extended Data Table 3). Adverse event reporting was according to the National Cancer Institute CTCAE Version 4.02. Performance status and overall survival was collected to death or censored at last clinical review; clinical data were anonymized once the data had been collated and verified by the sponsor. Drug dosing was at 400 mg of the oral PI3Kδ inhibitor AMG319 (15 patients) and, after an independent safety review, dosing at 300 mg in 6 patients; all patients who had at least 4 doses of the drug were

included in the final analyses. The study was discontinued after 30 patients had been dosed with AMG319 or placebo, thus limiting the clinical information on outcomes that can be gained from this trial. All patients had tissue collected as a dedicated research biopsy after consent and prior to randomization, with an additional sample collected during surgical resection. Tumor tissue was obtained fresh on the day of biopsy/surgery and a sample was immediately snap frozen. A proportion of the tumor tissue was cryopreserved in freezing medium (90% human AB serum and 10% DMSO) for subsequent analyses or, alternatively, directly disaggregated using a combination of enzymatic and mechanical dissociation for immediate analysis by FACS or cryopreservation as a single cell suspension, as previously described[50]. Blood samples were collected during the course of the study from which plasma and PBMCs were collected. PBMCs were isolated by centrifugation over lymphoprep$^{TM}$ (Axis-Shield PoC AS). RNA-seq data from a cohort of 39 consecutively collected HNSCC tumour samples (described in Ref [40]) was used to contextualise the immune profile of the HNSCC samples collected in the study (data available in Gene Expression Omnibus, accession number GSE72536).

**Histology and Immunohistochemistry**

Double immunostaining for CD8 and FOXP3 was performed on a Leica Bond RX platform, with antigen retrieval performed for 20 min at 97°C Bond ER2 antigen retrieval solution. Primary antibodies were incubated for 30 mins at room temperature (FoxP3 - Abcam: Clone 236A/E7 1:100 dilution; CD8 - DAKO: Clone C8/144B 1:50 dilution) and detected using the Leica Refine Polymer brown and red detection systems. Analysis was performed by two independent and blinded head & neck pathologists counting intratumoral $CD8^+$ and $FoxP3^+$ TIL in multiple random high-power fields (HPF) at magnification x200. Where possible, 10 HPF were counted.

**PK of AMG319**

50 µL of thawed plasma samples were mixed with 300 µL of Extraction Solution (100ng/mL [2H3, N15]-AMG 319 in methanol), centrifuged at 10,000g/RCF for 5 minutes to precipitate

the plasma proteins. The supernatant was transferred to a UPLC vial and placed on the autosampler (maintained at 8°C) for analysis. A freshly prepared calibration curve in the range 1-1000 ng/mL and frozen QC samples at 10, 100, 500 and 1000 ng/mL (K2 EDTA human plasma spiked with AMG 319) were analysed alongside each batch of patient samples. 5 µL of supernatant was injected into the UPLC-MS/MS system, configured with a Waters Acquity UPLC and Waters Quattro Premier XE mass spectrometer. Analytes were separated on an Acquity UPLC BEH C18 1.7µm (2.1 mm x 100 mm) column with a mobile phase flow rate of 0.3 mL/min. Mobile phase was composed of water, acetonitrile and formic acid. Analytes were detected using the multiple reaction monitoring (MRM) mode of the MS/MS system, operating in positive ion electrospray mode. MRMs were set up at m/z 386.4>251.3, 386.4>236.6, 251.3>251.3 and 251.3>236.3 for AMG 319 and at m/z 390.5>254.4 for [2H3, N15]-AMG 319. MassLynx software (version 4.1, Waters Ltd.) was used to control the instrumentation and for analysis of the peaks of interest and processing of spectral data.

**Anti-tetanus ELISA**

Anti-tetanus vaccine responses were measured in the plasma of patients (triplicate) by ELISA against tetanus toxoid (NIBSC, UK). A tetanus reference standard (NIBSC, UK) was used to quantitate the anti-tetanus IgG levels with a 2-fold increase over the baseline level used to determine a positive response to vaccine. In brief, 96 well MaxiSorp plates (Nunc, Denmark) were coated overnight with tetanus toxoid, washed with PBS-Tween prior to blocking with 1% milk (Marvel). A titrated reference standard (NIBSC), and diluted patient plasma samples (taken on day 1, 8 (day of vaccination), 15, 22 and off study) were incubated on the plates for 1hour, 37˚C. Detection was by addition of goat anti-human IG (Fc) antibody conjugated with horse-radish peroxidase (Sigma) for 1h, followed by o-phenylenediamine substrate (Sigma). Absorbance was read at 490nm.

**Anti-tetanus ELISpot**

Clear Multiscreen 96-well ELISPOT plates (Millipore, MAIPS4510) were pre-coated with 15 µg/ml anti-human IFNγ antibody (mAb 1 D1 K, Mabtech), and left overnight at 4°C. Thawed

PBMCs (2 x105 /well) were incubated in triplicate for 40 h at 37°C, 5% CO2 with medium only, 20µg/ml tetanus toxoid (NIBSC) or 5µg/ml PHA (Sigma). IFNγ secreting memory T-cells specific for tetanus were detected as spots using 1 µg/ml biotinylated IFNγ antibody (mAb 7B61 biotin, Mabtech) followed by 1 µg/ml streptavidin alkaline phosphatise (Mabtech) and a BCIP/ NBT detection kit (Zymed). A positive response to the vaccine was determined using an on-line algorithm, run DFR, Distribution Free Sampling (http://www.scharp.org/zoe/runDFR/).

**pAkt measurement**

Whole blood samples (10 ml) were collected in sodium heparin tubes pre-dose and 4 h post dose on days 1 and 15 for the first 11 patients (day 8 and 15 for the remaining 19 patients). Blood was stimulated with double-diluted anti-IgD (25-0.008 µg/ml) in deep well plates for 5 min. Blood was then lysed and fixed with BD PhosFlow Lyse/Fix buffer. Cell pellets were washed and then stored at -80°C until all samples from the same patient were ready for further analysis. Upon thawing, cells pellets were incubated with anti-human CD3-FITC and CD14-FITC, washed PBS+1%FBS, permeabilised with 80% MeOH and washed again before intracellular staining with CD20-PE Cy7 and pAkt (S473). Stained cell pellets were washed again before staining with a secondary antibody (anti-rabbit Alexa 647). Events were subsequently acquired on a Canto II flow cytometer (BD), and analysed using FACS Diva. MFI of pAkt in B cells was plotted against the anti-IgD concentration. The AUC was calculated and a drop of 50% in AUC between pre- and post-dose was validated to be the result of drug inhibition.

**Tumor transcriptome analysis**

Cryosections (10 µm) were cut from snap frozen tumor and RNA was extracted using the Maxwell® RSC instrument and Maxwell® RSC SimplyRNA Tissue kit (Promega, Southampton, UK), according to the manufacturer's instructions. RNA was quantified using the Qubit fluorometer (ThermoFisher Scientific) and quality was assessed using the Agilent 2100 Bioanalyzer generating an RNA integrity number (RIN; Agilent Technologies UK Ltd.).

RNA sequencing was performed by Edinburgh Genomics (Edinburgh, UK.); mRNA libraries were prepared using the TruSeq Stranded Total RNA Library Prep Kit (Illumina) and paired-end sequenced (100bp) on the NovaSeq 6000 platform (Illumina) to yield an average read depth of $40x10^6$ reads. Reads were mapped to hg19 reference genome using STAR with our in-house pipeline (https://github.com/ndu-UCSD/LJI_RNA_SEQ_PIPELINE_V2). A total of 22 paired (14 from treatment and 8 from placebo group) samples with at least 70 percent of mapping reads were selected. Differential expression analysis between the pre and post treatment, as well as between pre and post placebo, was performed using DESeq2 (v1.24.0). The threshold for differentially expressed genes was determined with fold change of > $\log_2$ 0.75 and an adjusted P-value < 0.1. Between treatment pre and post, 93 genes were identified as significant, whereas 3 genes were significant between placebo pre and post. Cells were dispersed from fresh tumor tissue and used immediately for flow cytometric analysis and cell sorting (method as below); staining used antibodies to human CD45 (HI30), CD3 (SK7), CD8 (SK1), CD4 (RPA-T4), CD19 (J3-119), CD20 (2H7), CD14 (MφP9) and HLA-DR (L243). $CD8^+$ T cells were bulk sorted into ice-cold TRIzol LS reagent[50] (Thermo Fisher Scientific) on a BD FACS Fusion (BD Bioscience). Reads from sorted CD8 RNA were mapped to hg19 reference genome using STAR with the same in-house pipeline as above. In total, we had 17 samples available, placebo (pre-2, post-3) and treatment (pre-6, post-6), out of which 3 were paired (1-placebo and 2-treatment). The differentially expressed genes between post treatment and remaining samples resulted in 455 significant genes (fold change of > $\log_2$ 0.75 and an adjusted P-value < 0.05).

**Flow cytometry**

Cells dispersed from cryopreserved tumor tissue or PBMCs isolated from peripheral blood were prepared in staining buffer (PBS with 2% FBS and 2 mM EDTA), FcR blocked (clone 2.4G2, BD Biosciences) and stained with antibodies as indicated below for 30 min at 4°C. Cell viability was determined using fixable viability dye (ThermoFisher).

Murine lymphocytes were isolated from the spleen by mechanical dispersion through a 70-µm cell strainer (Miltenyi) to generate single-cell suspensions. RBC lysis (Biolegend) was performed to remove red blood cells. Tumor samples were harvested and lymphocytes were isolated by dispersing the tumor tissue in 2 ml of PBS, followed by incubation of samples at 37°C for 15 min with DNase I (Sigma) and Liberase DL (Roche). The suspension was then diluted with MACS buffer and passed through a 70-µm cell strainer to generate a single cell suspension. Colons were collected and rinsed in 1mM dithiothreitol (DTT) to remove feces. Each colon was cut into 2-3mm pieces and incubated 3 times in pre-digestion solution (HBSS containing 5% FBS and 2mM EDTA) at 37°C for 20 min under high rotation to remove epithelial cells. Then tissues were minced with scissors and incubated with digestion solution (HBSS containing 5% FBS, 100 μg/ml DNase I (Sigma) and 1 mg/ml collagenase (Sigma)) at 37°C for 20 min under high rotation to get single cell solutions of lamina propria cells. Cells were prepared in staining buffer (PBS with 2% FBS and 2 mM EDTA), FcR blocked (clone 2.4G2, BD Biosciences) and stained with antibodies as indicated below for 30 min at 4°C; secondary stains were done for selected markers. Samples were then sorted or fixed and intracellularly stained using a FoxP3 transcription factor kit according to manufacturer's instructions (eBioscience). Cell viability was determined using fixable viability dye (ThermoFisher). The following antibodies from BD Biosciences, Biolegend, Miltenyi or eBbioscience were used: anti-human PD-1 (EH12.1), CD4 (OKT4), CD137 (4B4-1), GITR (108-17), ICOS (C398.4A), CD8A (SK1), CD25 (M-A251), CD3 (SK7), CD127 (eBioRDR5), CD45 (HI30), CD14 (HCD14), CD20 (2H7); anti-mouse Cd3 (145-2C11), Cd4 (RM4-5), Cd8 (53-6.7), Ki67 (B56), Tox (REA473), Cd19 (6D5), Cd45 (30-F11), FoxP3 (FJK-16s), GzmB (QA16A02). All samples were acquired on a BD FACS Fortessa or sorted on a BD FACS Fusion (both BD Biosciences) and analyzed using FlowJo 10.4.1 for subsequent single-cell RNA-seq analysis.

**Single-cell transcriptome analysis**

For human tumor, single-cell RNA-seq was performed by Smart-seq2 as previously described[51]. Reads were mapped with our in-house pipeline as above. Good quality cells were defined as those with at least 200 genes, at least 60 percent of mapping reads, mitochondrial counts of at most 20 percent, at least 50,000 total counts (reported by STAR excluding tRNA and rRNA), and a 5' to 3' bias of at most 2. Filtered cells were analyzed using the package Seurat (v3.1.5). In order to separate CD4 and CD8 more effectively, we performed Differential gene expression analysis between single-positive cells using CD4 and CD8B genes. Cells were clustered using 178 significant genes (adjusted *P*-value < 0.5).

For murine single-cell RNA-seq, we used the 10x platform (10x Genomics, Pleasanton, CA, USA) according to the manufacturer's instructions. Reads were mapped with Cell Ranger followed by our in-house QC pipeline (https://github.com/vijaybioinfo/quality_control) and demultiplexed with bcl2fastq using default parameters. Cell Ranger aggr routine was used and CITE-seq data was processed using our custom pipeline (https://github.com/vijaybioinfo/ab_capture). Briefly, raw output from Cell Ranger is taken and cell barcodes with less than 100 UMI counts as their top feature are discarded, the remaining barcodes are classified by *MULTIseqDemux* from Seurat. Finally, cell barcodes where the assigned feature doesn't have the highest UMI count are fixed, and cells with a fold change of less than 3 between the top two features are reclassified as doublets. Before clustering, cells were filtered for at least 300 at most 5000 genes, at least 500 and at most 10000 UMI counts, and at most 5 percent of mitochondrial counts. Cell types were identified using Seurat's *FindAllMarkers* function. Differential expression was calculated with MAST[52] (v1.10.0) DESeq2 (v1.24.0) as previously described[51] and genes with an adjusted *P*-value < 0.05 and a fold change of > $\log_2$ 0.5 were defined as significant. GSEA scores were estimated with fgsea (v1.10.1) in R using signal-to-noise ratio as the metric (minSize = 3 and maxSize = 500). Enrichment scores were shown as GSEA plots. Signature scores were computed using Seurat's *AddModuleScore* function with default parameters. In short, the score is defined for each cell by subtracting the mean expression of an aggregate of control gene lists from the

mean of the signature gene list. Control gene lists were randomly selected (same size as the signature list) from bins delimited based on the level of expression of the signature list.

**T-cell receptor analysis**

TCR were reconstructed from single-cell RNA-seq reads using MiXCR with default parameters. Then, shared TCR were defined by having the same CDR3 sequence in both the alpha and beta chains and coming from the same donor. Enriched TCR were defined as those with a frequency higher or equal to two. Lastly, TCR network plots were generated using the Python package *graphviz*.

**Accession codes**

Sequencing data has been uploaded onto the Gene Expression Omnibus (accession code GSE166150). Access for reviewers can be found using the password utqpmasoplopdwz

**Quantification and statistical analysis**

The number of subjects, samples or mice/group, replication in independent experiments, and statistical tests can be found in the figure legends. Details on quality control, sample elimination and displayed data are stated the method details and figure legends. Sample sizes were chosen based on published studies to ensure sufficient numbers of mice in each group enabling reliable statistical testing and accounting for variability. RNA-seq samples that didn't pass quality control weren't included in the analyses. Experimental results were reliably reproduced in at least two independent experiments. Animals of same sex and age were randomly assigned to experimental groups Statistical analyses were performed with Graph Pad Prism 9 and statistical tests used are indicated in the figure legends and experimental model and subject details.

# Figures

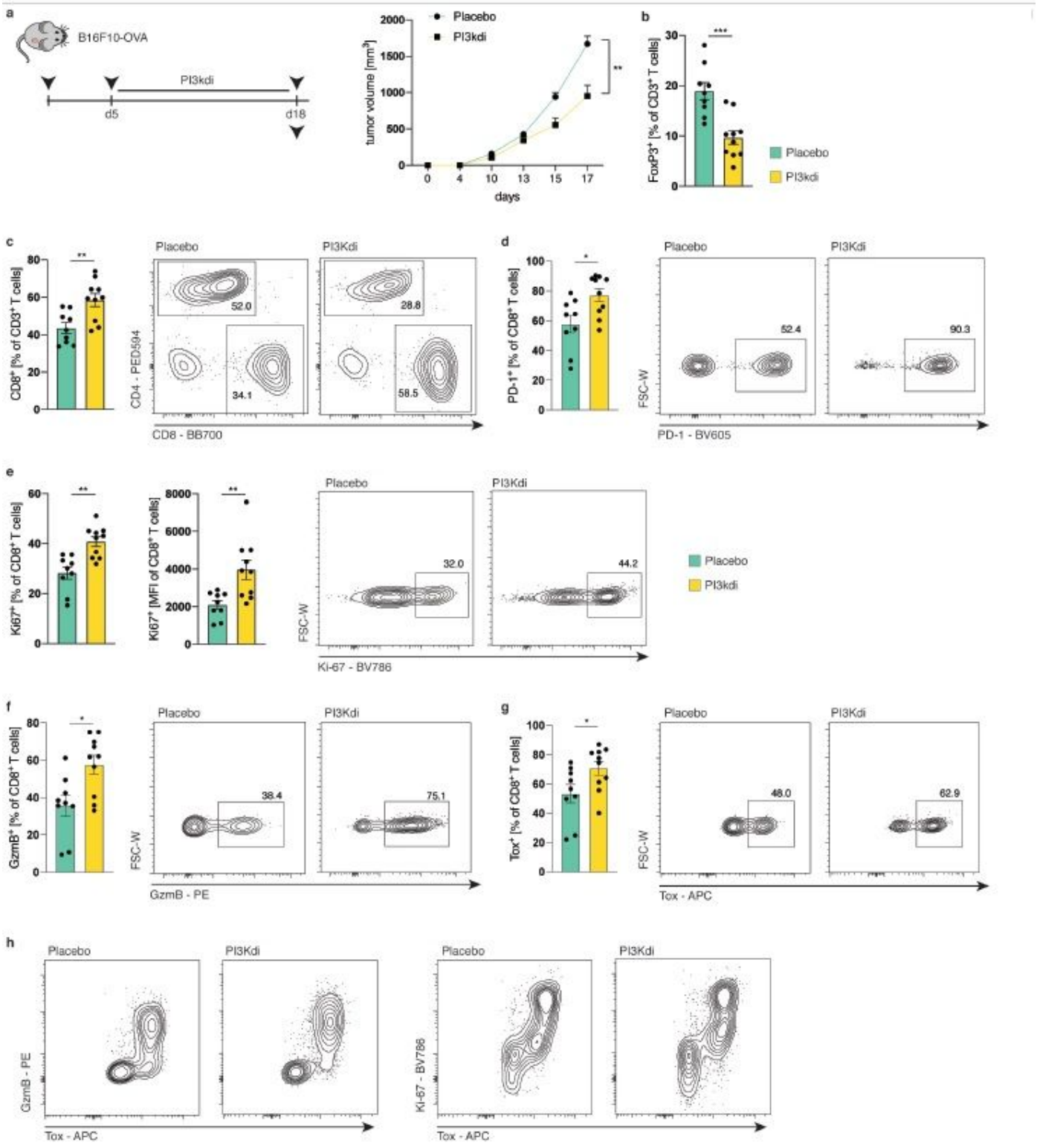


**Figure 1**

PI3Kδ-inhibition induces are pro-inflammatory tumor microenvironment a, Mice were inoculated s.c. with B16F10-OVA cells and fed either a control diet or a diet containing the PI-3065 PI3Kδ inhibitor for the indicated treatment period. Tumor volume (a) and flow-cytometric analyses of cell frequencies (b-g) of

mice treated as indicated. h, Shown are representative contour plots of intratumoral CD8+ T cells depicting the indicated markers. n=9-10 mice/group. Data are mean +/- S.E.M. Significance for comparisons were computed using Mann-Whitney test are the data are representative of two independent experiments.

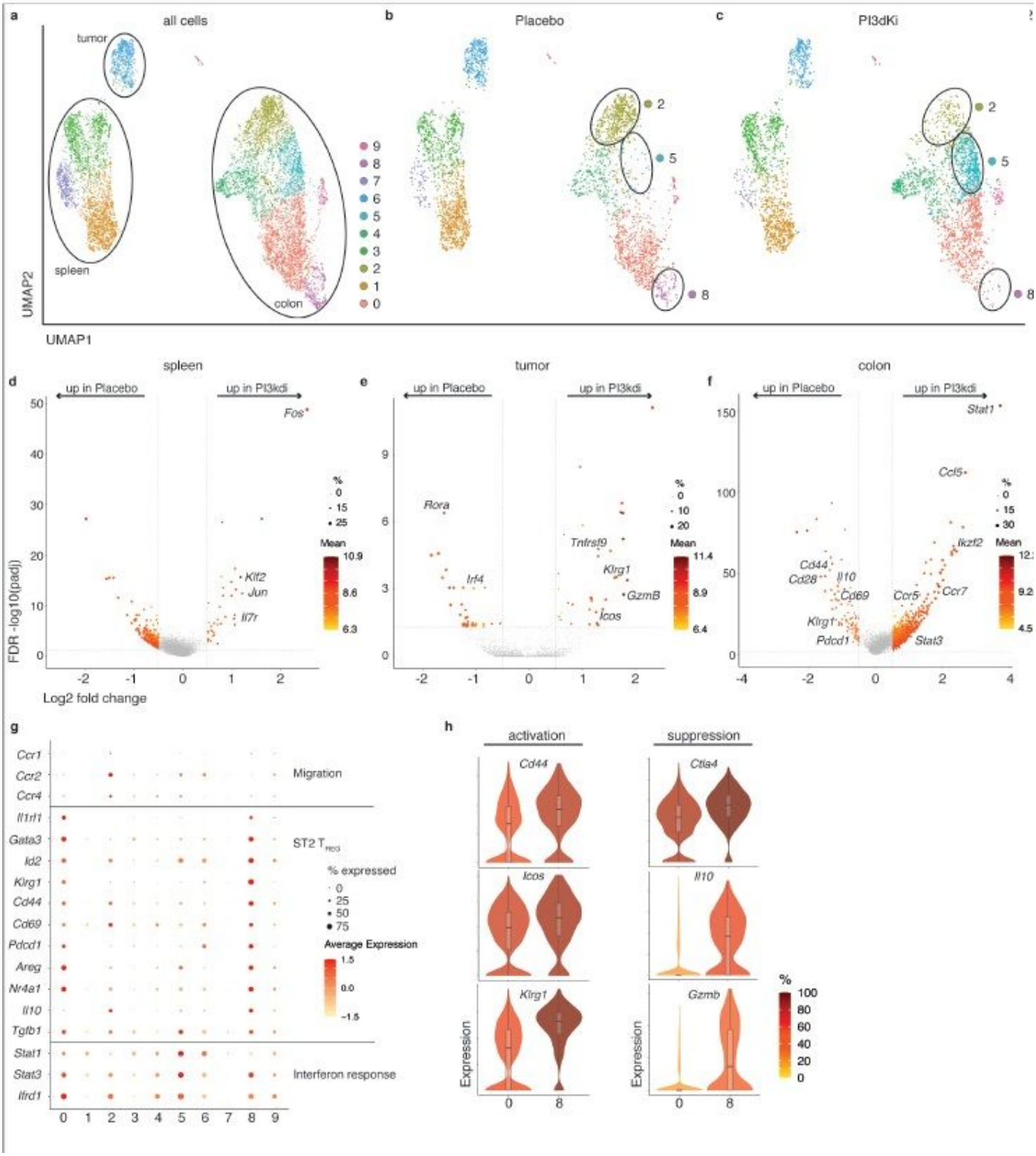


**Figure 2**

PI3Kδ inhibition affects distinct TREG cell subtypes a-c, Analysis of 10x single-cell RNA-seq data displayed by UMAP analysis. Seurat clustering of FoxP3+CD4+ T cells independent of treatment (a), in placebo-treated control mice (b) and PI-3065-treated mice (c). d-f, Volcano plots of single-cell RNA-seq analysis of placebo-treated control mice and PI-3065-treated mice in spleen (d) tumor (e) and colon (f). Highlighted are transcripts with a >0.5 log2 fold change. g, Curtain plot highlighting selected genes in each cluster with average transcript expression (color scale) and percent of expressing cells (size scale). h, Violin plots showing normalized expression levels (log2(CPM+1)) of highlighted genes in cluster 0 and cluster 8

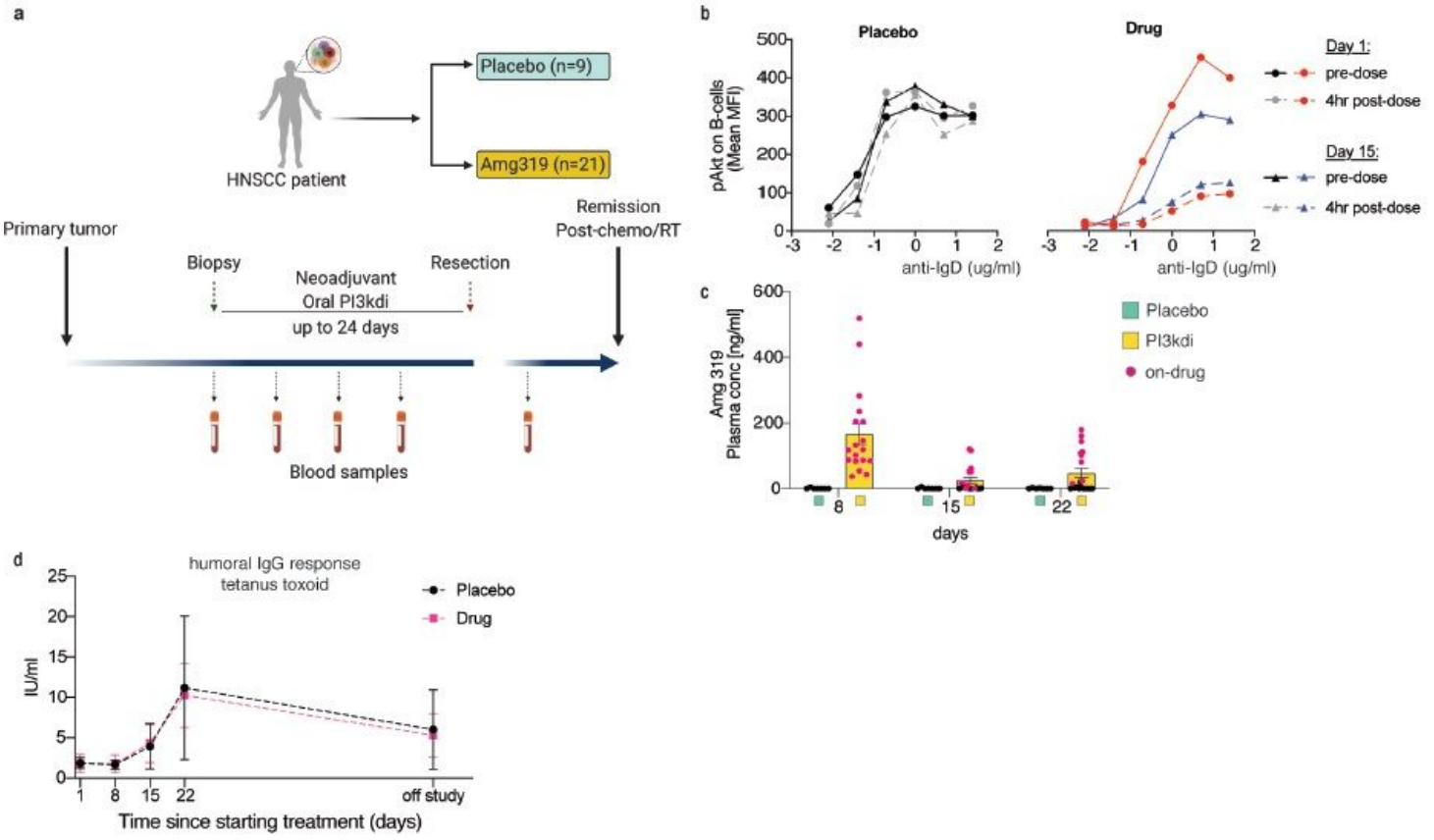


## Figure 3

AMG319 causes significant immune related adverse events a, Trial schematic of the placebo-controlled dose escalation study. b, Assessment of the level of AKT phosphorylation in B cells at indicated time points pre-dose and 4h after treatment with AMG319, data from one representative patient are shown. c, Plasma concentrations of AMG319 in placebo-controlled and drug-treated patients at indicated time points. Highlighted in red are patients who were either on-treatment or had only recently (2 days prior to analysis) or briefly discontinued treatment. d, Evaluation of the humoral immune response to tetanus vaccination (day 8) using ELISA.

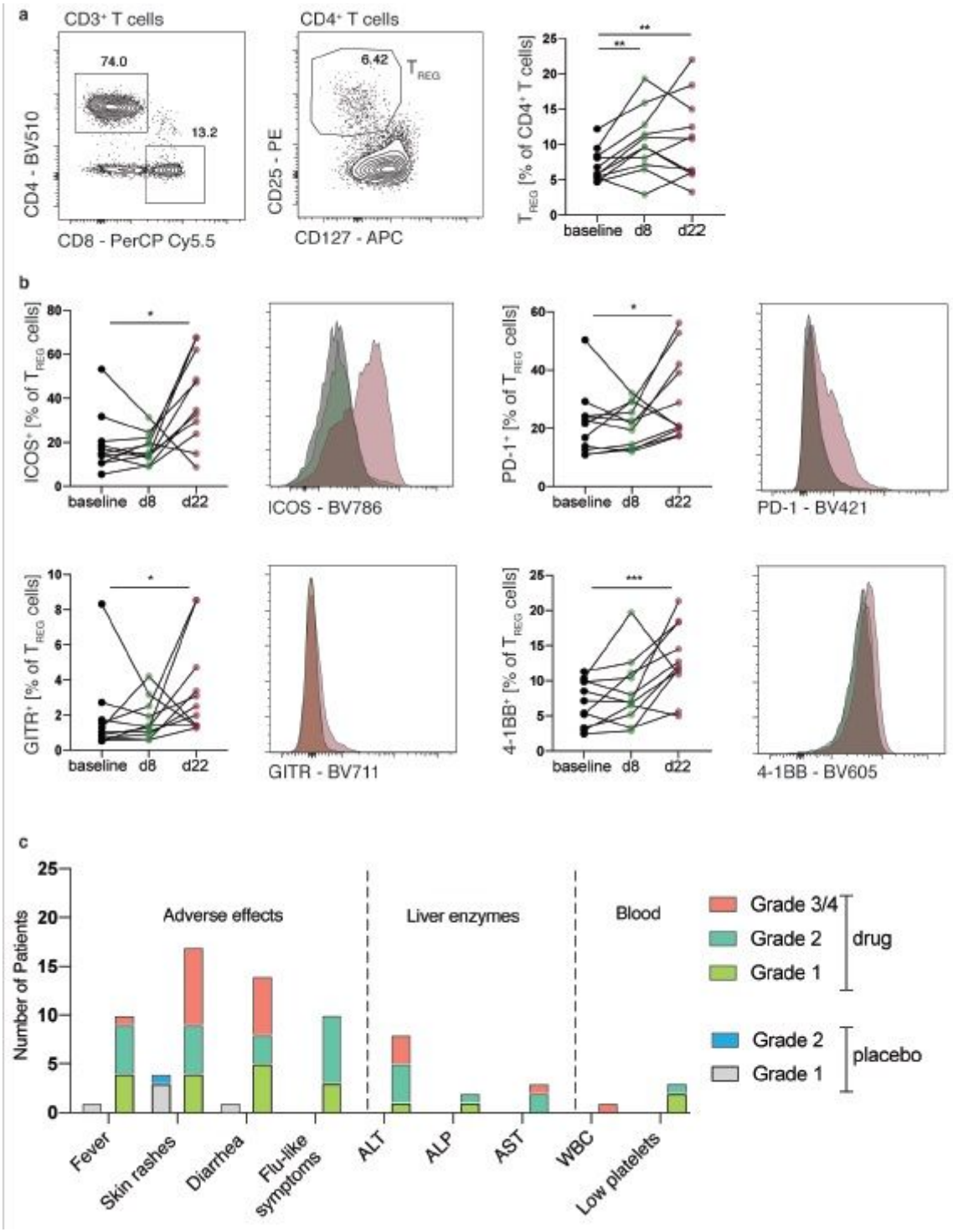


## Figure 4

AMG319 displaces activated TREG cells into circulation a,b, Representative contour plots of CD3+ T cells and TREG cells and flow-cytometric analyses of the frequency of (a) and expression of activation markers (b) in circulating TREG cells in AMG319-treated patients at indicated time points. c, Frequency, type and severity of observed immune related adverse events in placebo and AMG319-treated patients. Data are mean +/- S.E.M. Significance for comparisons were computed using Wilcoxon matched-pairs signed rank test (a,b).

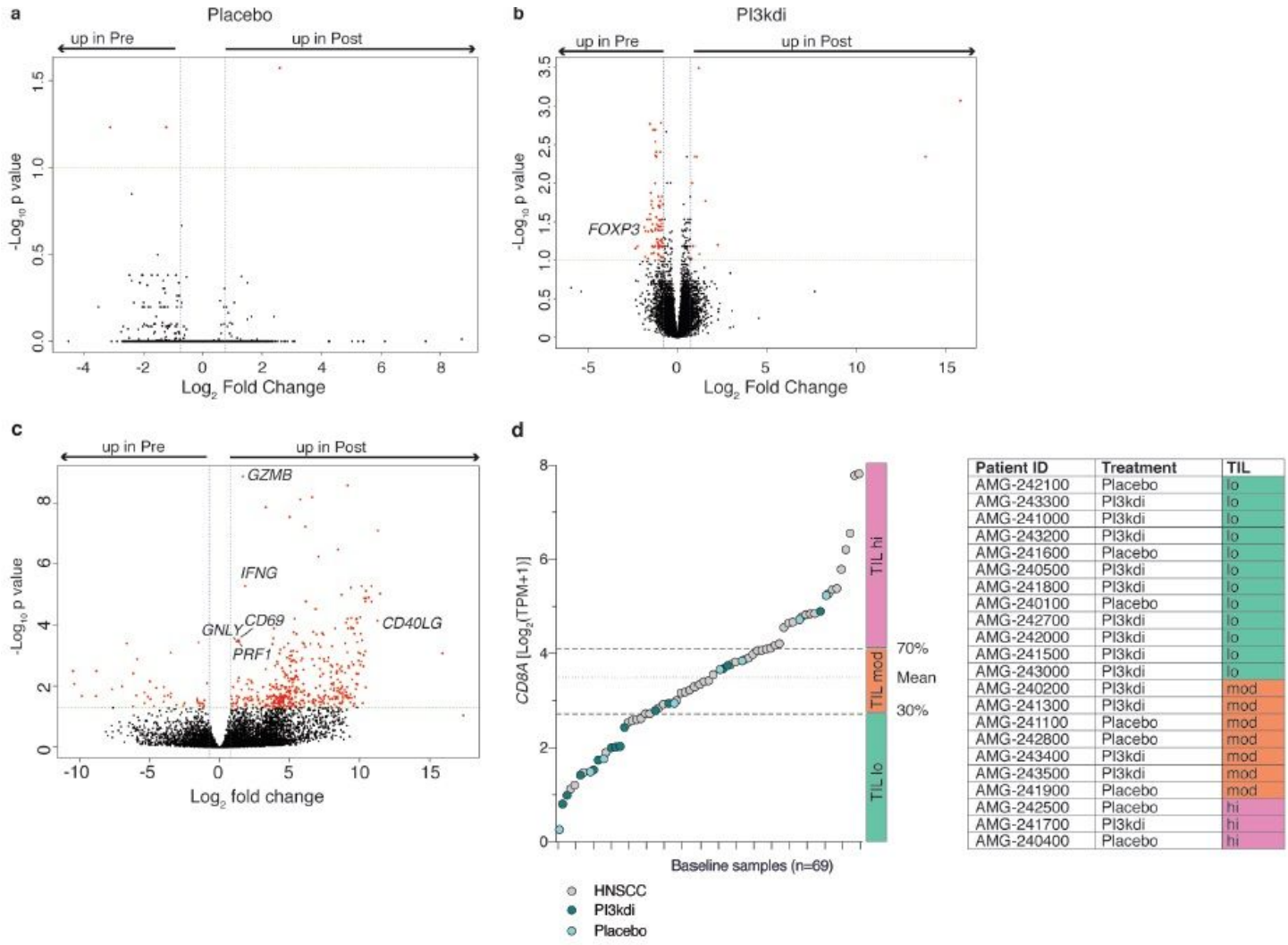


| Patient ID | Treatment | TIL |
|---|---|---|
| AMG-242100 | Placebo | lo |
| AMG-243300 | PI3kdi | lo |
| AMG-241000 | PI3kdi | lo |
| AMG-243200 | PI3kdi | lo |
| AMG-241600 | Placebo | lo |
| AMG-240500 | PI3kdi | lo |
| AMG-241800 | PI3kdi | lo |
| AMG-240100 | Placebo | lo |
| AMG-242700 | PI3kdi | lo |
| AMG-242000 | PI3kdi | lo |
| AMG-241500 | PI3kdi | lo |
| AMG-243000 | PI3kdi | lo |
| AMG-240200 | PI3kdi | mod |
| AMG-241300 | PI3kdi | mod |
| AMG-241100 | Placebo | mod |
| AMG-242800 | Placebo | mod |
| AMG-243400 | PI3kdi | mod |
| AMG-243500 | PI3kdi | mod |
| AMG-241900 | Placebo | mod |
| AMG-242500 | Placebo | hi |
| AMG-241700 | PI3kdi | hi |
| AMG-240400 | Placebo | hi |

## Figure 5

AMG319 treatment changes the cellular composition of the tumor microenvironment a-c Volcano plots of whole tumor RNA-seq analysis (a,b) or bulk RNA-seq analysis of CD8+ T cells (c) comparing AMG-319 to placebo treated patients. Differentially expressed genes between pre and post-treatment samples are highlighted in red. Depicted are transcripts that change in expression more than 0.75-fold and adjusted P value of ≤ 0.1 (a,b) or <0.05 (c). d, Stratification into TIL status (TIL lo, TIL mod, and TIL hi) from samples of patients enrolled in this study in comparison to a previously published HNSCC cohort.

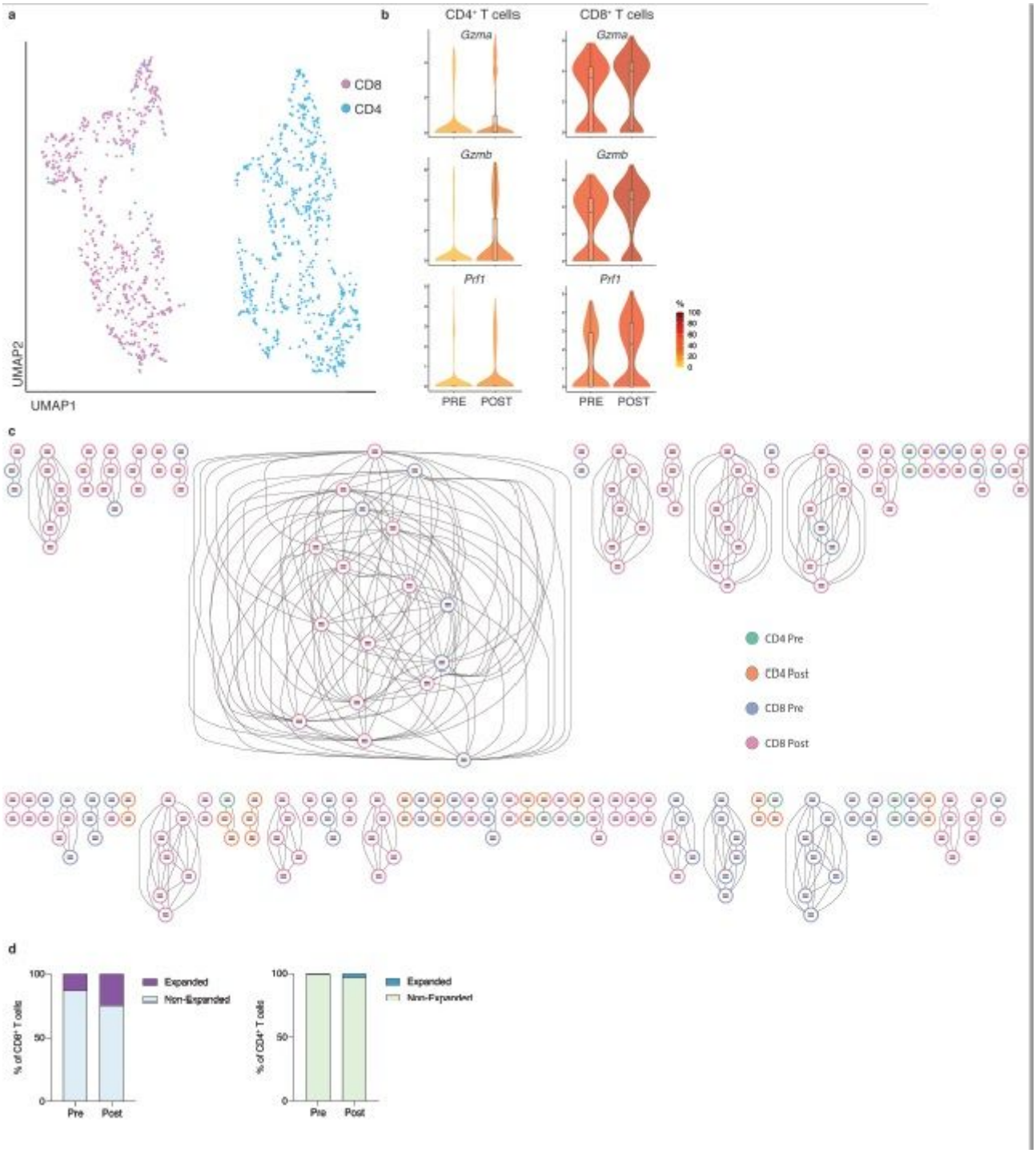


## Figure 6

Single-cell RNA-seq analysis reveals substantial oligoclonal expansion of tumor-infiltrating CD8+ T cells post-treatment a, Analysis of smart-seq2 single-cell RNA-seq data of sorted tumor-infiltrating CD3+ T cells displayed by UMAP analysis. b, Violin plots depicting the expression of differentially expression highlighted genes in CD4+ T cells (left) or CD8+ T cells (right). c, TraCer plots of all clonally expanded CD4+ and CD8+ T cells (=/>2 clonotypes) in pre- and post-treatment samples of AMG319-treated patients. d, Percentages of non-expanded and expanded CD8+ and CD4+ T cell clones in pre- versus post-treatment samples.

# Supplementary Files

This is a list of supplementary files associated with this preprint. Click to download.

- ExtendedDataTable1.xlsx
- ExtendedDataTable2.xlsx
- ExtendedDataTable3.xlsx
- ExtendedDataTable4.xlsx
- ExtendedDataTable5.xlsx
- ExtendedDataTable6.xlsx
- ExtendedDataFigure1.jpg
- ExtendedDataFigure2.jpg
- ExtendedDataFigure3.jpg
- ExtendedDataFigure4.jpg